BULLETIN OF THE POLISH ACADEMY OF SCIENCES
TECHNICAL SCIENCES, Vol. 70(6), 2022, Article number: e143648
DOI: 10.24425/bpasts.2022.143648

Experimental investigation of Euler's elastica: in-situ SEM nanowire post-buckling

Aleksandra MANECKA-PADAŻ[1]*, **Piotr JENCZYK**[1], **Ryszard B. PĘCHERSKI**[1], and **Anna NYKIEL**[2]

[1] Institute of Fundamental Technological Research Polish Academy of Sciences, Poland
[2] Institute of Nuclear Physics Polish Academy of Sciences, Poland

Abstract. An in-situ nanoindenter with a flat tip was employed to conduct buckling tests of a single nanowire with simultaneous SEM imaging. A series of SEM images allowed us to calculate deflection. The deflection was confronted with the mathematical model of elastica. The post-buckling behaviour of nanowires is conducted in the framework of the nonlinear elasticity theory. Results show the significant effect of geometrical parameters on the stability of buckled nanowires.

Key words: post-buckling; nanowire; nanomechanics.

1. INTRODUCTION

The Euler Buckling Formula (EBF), which gives the critical value of the compressive load required to buckle a long slender rod, is widely used mainly by structural and mechanical engineers [1]. Jacob Bernoulli formulated (1691) the elastica problem, and, about fifty years later, Daniel Bernoulli discovered the related energy functional stating the minimal principle of elastica. The problem was solved by Leonhard Euler (1744) [2]. Currently, it is known as the elastica theory. It presents enormous potential as an interesting issue for mathematicians (dynamics of a pendulum analogy), engineers (designing), and historians of mathematics (development of elliptic functions), [1]. The load at which loss of stability and bifurcation occurs is the critical buckling load. The deflection path after bifurcation is called the post-buckling path [3].

EBF finds practical applications on the macroscopic level, e.g. in deep-sea cable and pipe laying operations [4], in mechanical engineering designing stable mechanisms [5], wind turbine towers design [6], and the behaviour of nitinol rods provides an excellent match with the elastica theory [7]. Also, Hiroshi Yoshihara and Makoto Maruta conducted buckling tests of slender wood elements in order to determine critical load using the elastica theory [8]. On the other hand, on the microscopic or nano-scale levels, the non-linear elastic stability processes become a subject of interest worth mentioning [8–11], as well as, in some areas of biomechanics, i.e. a model for the DNA writhing [12, 13]. It is also demonstrated that for a small radius of the nanotubes the buckling mode falls into the regime of Euler beam buckling [14].

*e-mail: amanecka@ippt.pan.pl

Manuscript submitted 2022-09-26, revised 2022-10-21, initially accepted for publication data3, published in 2022-10-25, published in December 2022.

In our view, a field for further, more adequate studies results from a better description that should account for scale and surface energy effects.

The increasing demand for nanomaterials with extraordinary properties, e.g. elastic ones, requires mechanical behaviour description. Microscopy measurements have significant meaning in examining the buckling of nanostructures. For instance, atomic force microscopy (AFM) is used to obtain the force-distance curve of nanotubes while buckling [9, 14, 15]. In situ transmission electron microscopy (TEM) also provides information on the characterisation of buckling [10]. The experimental investigation of buckling on the nanoscale is challenging due to the troublesome manipulation at such a small scale. The examination of the various characteristics of nanostructures such as optical and electrical ones [16, 17], magnetic properties [18], vibration analysis [19], energy absorption [20, 21], or viscoelastic behaviour [18]. Several studies have been conducted to analyse the buckling of the nanostructures, i.e. [9, 22, 23]. Setoodeh *et al*. presented an exact analytical and efficient expression for the post-buckling configurations of single-walled carbon nanotubes (CNTs) [22]. The analytical and numerical solutions were obtained for the nonlinear post-buckling problem. Finally, the nonlocal theory was presented, and a solution for various nonlocal parameter values was introduced. Thongyothee and Chucheepsakul [23] investigated the post-buckling configurations of a nanorod. Based on the elastica theory, the governing equations of nanorods, including both nonlocal elasticity and surface stress, were presented [23]. The results show that nanorods with the nonlocal elasticity effect undergo increasingly large deformation. In the studies mentioned above, researchers mainly concentrated on numerical analysis. However, a relatively small number of papers focus on the experimental confirmation of modelling results. For example, Obrokhotov *et al*. measured the buckling of Ag-Ga nanoneedles grown on AFM tip [15]. The measurements include AFM force-distance curves. The comparison of exper-

imentally measured buckling of a nanoneedle with the elastica model was carried out using the generalised elastica approach. The resulting best-fit F-D curve varies with the changes in the value of Young's modulus. The method facilitates providing an estimate of Young's modulus. However, the deflection measurement in various states of post-buckling is not calculated. Pathak *et al*. reported on the mechanical behaviour of a dense brush of small-diameter (1–3 nm) carbon nanotubes (CNTs) [14].

Under compression with spherical indenters of different radii, CNT brushes exhibit a higher modulus ($\sim 17-20$ GPa) and orders of magnitude higher resistance to buckling than vapour phase deposited CNT brushes or carbon walls. Although the discussion above provides essential information about the buckling behaviour of 1D nanostructures, there is no exact characterisation of the bifurcation process. The demonstrated paper results of SEM observations attempt to fill this gap, at least partially. Then, SEM images are used to obtain normalised displacement-deflection curves of post-buckled nanowires. The results are the subject of analysis vis-à-vis Euler's elasticas.

2. MATERIALS AND METHODS

The manufacturing process should be designed and elaborated to fulfil the EBF application perspective for nanostructural instability analysis. Therefore, we describe how the forest-like structure of Co nanowires can be fabricated and investigated. For instance, an in-situ nanoindenter may be employed for a single nanowire buckling test with in situ SEM imaging. The proposed procedure results in three steps:

(a) electrodeposition of metal in the porous membrane,
(b) dissolution of the template to unveil metal nanowires,
(c) compression of a single nanowire with the use of a flat tip nanoindenter.

Figure 1 shows the production of the Co nanowire arrays by template-assisted electrodeposition. The commercially available polycarbonate (PC) membranes purchased at Sterlitech Corporation were used as a template. One side of the PC membranes was covered with an Au layer (300 nm) to close the pores and provide electrical contact for the non-conductive membrane, which served as a working electrode. The process was performed at a three-electrode setup with a platinum sheet and Ag/AgCl as a counter and the reference electrodes. We used the membranes with a pore diameter of 50 nm and a thickness of 6 μm, which determined the nanowire diameter and maximal length. The process was performed at the potentiostat mode at a cathodic potential equal to –1 V vs Ag/AgCl. Potentiostat AUTO LAB PGSTAT302N controlled it with the current accuracy of 0.01 μA. Before the nanowire growth, the membranes were wetted in distilled water while the counter electrode was ultrasonically cleaned. The electrolyte was composed of 0.50 M $CoSO_4$ $7H_2O$ and 0.65 g/l H_3BO_3 and prepared from chemicals of analytical grade and deionised water (resistivity > 18 MΩ cm) from the Millipore system. The electrolyte temperature was kept at 25°C with pH $= 3.8$ adjusted using diluted H_2SO_4 and NaOH. The nanowire length was controlled by deposition time, and the electrical charge was reduced into the nanochannels, or one of these factors played the controlling role.

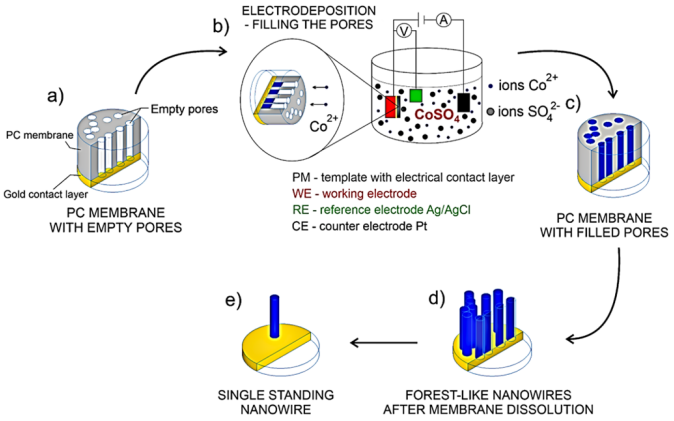

Fig. 1. Single Co nanowire production: a) Cross-section of polycarbonate (PC) membrane: empty pores in membrane with pre-sputtered gold contact layer; b) template-assisted electrodeposition process of Co nanowires in electrochemical cell with a three-electrode system; c) filled pores in PC membrane – formed nanowires; d) forest-like Co nanowires after membrane dissolution attached to gold layer as substrate; e) single standing Co nanowire after FIB-milling of its vicinity

To receive free-standing nanowires, we dissolved the polycarbonate membrane using dichloromethane. The scanning electron microscopy (SEM) images revealed a matrix of nanowires as a forest-like structure. The nanowires were left up to solvent evaporation to avoid damage and deviation from the perpendicular direction caused by dichloromethane flow.

Investigation of the as-obtained nanowire was performed using a ZEISS Crossbeam 350 scanning electron microscope (SEM) equipped with an in-situ Alemnis nanoindenter with a flat tip of diameter 5 μm. The Series of SEM images were taken during the buckling, and deformation was observed. Images were saved with constant time intervals. Total deformation was measured by comparison with the scale provided by SEM software in horizontal and vertical directions. The nanowires mounted in the nanoindenter are perpendicular to the electron beam direction. The SEM table is then tilted to 15 degrees to enable observation and precise tip movement. Therefore, 15 degrees SEM table tilt was taken into account for the vertical direction, and measured wire end displacement was divided by cos (15°) to obtain the actual distance. There was no such need for the horizontal direction. Measured deflection and corresponding nanowire end displacement were compared with mathematical models of elastica. The force was not measured due to experimental hardware limitations. For the procedure described above, there are a couple of factors causing measurement uncertainty: (a) due to one direction of observation, it is not clear how precisely the pre-compressed nanowire is perpendicular to the substrate; (b) due to one direction of observation, it is not clear what the exact direction of maximal deformation is; (c) for length and diameter measurements, it is not clear at which point there is a substrate – nanowire transition. Therefore, the sample was observed in SEM from various directions to find a wire as vertical as possible. The marker was made with a focused ion beam (FIB) to enable identifying the wire of interest. After nanowire compression, the sample was again observed with SEM to acquire the direction of deformation. Finally, the diameter was measured at

the ends and in the middle of the nanowire. The measurements were made three times, and an average with standard deviation was calculated.

3. APPLICATION OF EULER'S ELASTICA THEORY

According to the Euler–Bernoulli beam theory, the nanowire is assumed to be a slender, elastic, incompressible beam of constant length l, simply supported. The concentrated compressive load F has been applied to the nanowire.

Figure 2 depicts the changes in the curvature of the nanowire due to the compression, α is the initial angle, u_1 wire end displacement and u_2 the mid-span deflection. The differential equation for the elastica at given point X [24]:

$$\theta''(s) + \lambda^2 \sin\theta(s) = 0, \tag{1}$$

where: θ is the angle of inclination of the tangent $\mathbf{t}$ to the elastica at X, s is the curvilinear coordinate and $s \in < 0, l >$, $\lambda = \sqrt{\frac{F}{B}}$ where F and B are force and bending stiffness, respectively. λ can be defined also as $\lambda = \frac{2mK(k)}{l}$ [24].

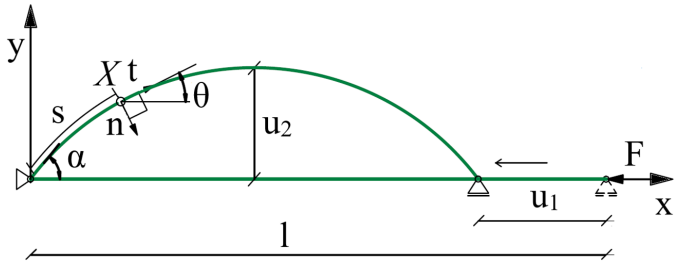

Fig. 2. The configuration of a nanowire due to the compression

For a simply supported beam, we can define the following boundary conditions:

$$\theta'(0) = \theta'(l) = 0. \tag{2}$$

The analytical solution of the geometrically nonlinear equation (2) is possible using the elliptic integrals and the final form of the solution is as follows [24]:

$$x = -s + \frac{2}{\lambda}\left\{E\left[am\left(s\lambda + K(k), k\right), k\right] - E\left[am\left(K(k), k\right)k\right]\right\}, \tag{3}$$

$$y = -\frac{2k}{\lambda} cn\left(s\lambda + K(k)\right), \tag{4}$$

where: x, y are coordinates and $x, y \in < 0, l >$, $E(x,k) = \int_0^x \sqrt{1 - k\sin^2 t}\,\mathrm{d}t$ is the incomplete elliptic integral of the second kind, $k = \sin\frac{\alpha}{2}$, $\alpha = \theta(0)$ and $0 \le \alpha \le \pi$, $K(k) = \int_0^{\frac{\pi}{2}} \frac{\mathrm{d}\phi}{\sqrt{1 - k^2\sin^2\phi}}$ is the complete elliptic integral of the first kind, $\phi = \arcsin\left(\frac{\sin\frac{\theta}{2}}{k}\right)$, $am(x,k)$ is the Jacobi amplitude function of modulus k, $cn(x,k) = \cos(am(x,k))$ is the Jacobi cosine amplitude function.

The displacement of the end of the wire can be expressed as [24]:

$$u_1(l) = 2l\left(1 - \frac{E(k)}{K(k)}\right). \tag{5}$$

The mid-span deflection can be evaluated as:

$$u_2(l/2) = \frac{kl}{mK(k)}, \tag{6}$$

where $m = 1, 3, 5, \ldots$

Figure 3 represents the relationship between the normalised mid-span deflection (u_2/l) and normalised displacement of the end of the nanowire (u_1/l). Various post-buckling shapes of elastica can be observed.

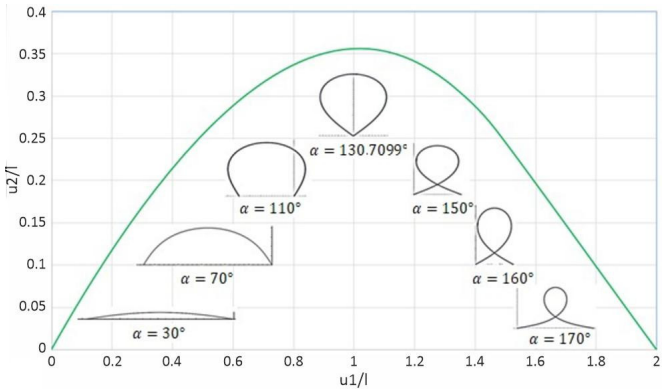

Fig. 3. The relationship between the normalised mid-span deflection (u_2/l) and normalised displacement of the end of the nanowire (u_1/l) together with various post-buckling shapes

4. RESULTS AND DISCUSSION

The experimental method of obtaining a relationship between nanowire end displacement and mid-span deflection is based on SEM images of buckling. The theoretical curve is received using equations (5) and (6). The nanowires viewed in the SEM chamber appear in the first bifurcation mode; therefore, $m = 1$ is considered. Figure 4 shows the mid-span deflection versus the displacement of the end of the nanowire. Results are presented for three various nanowires with different length to diameter ratios $\left(\frac{l}{d}\right)$, namely, nanowire a: $\frac{l}{d} = 12.8$; nanowire b: $\frac{l}{d} = 28.4$; nanowire c: $\frac{l}{d} = 46.3$. The dimensions of tested nanowires are $l_a = 0.835$ µm, $d_a = 0.065$ µm; $l_b = 2.648$ µm, $d_b = 0.093$ µm; $l_c = 4.185$ µm, $d_c = 0.090$ µm.

The maximum displacement of the end of the nanowire is the largest for nanowire a and $\delta l_{a\max} = \frac{u_1}{l_a} = 0.557$ while the other nanowires reach values $\delta l_{b\max} = \frac{u_1}{l_b} = 0.367$ and $\delta l_{c\max} =$

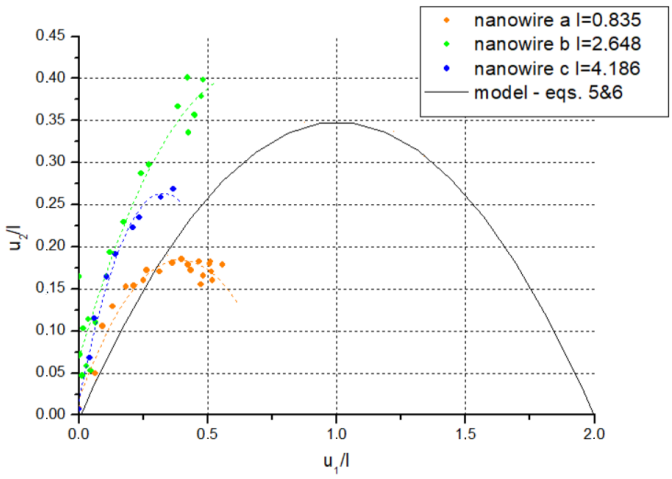

Fig. 4. Elastica-determined u1/l-u2/l curves and experimental results

$\frac{u_1}{l_c} = 0.475$. The maximum mid-span deflection value in the case of the nanowire a was reached quite fast and remained on a similar level until the end of the experiment. In this case, the experimental deflection was quite close to the theoretical one. Higher values of u_1 and consequently u_2 were obtained due to a no longer satisfied assumption of sliding joint at the moving end of the nanowire. Therefore, it is very complicated to maintain the same boundary conditions in the practical test as in the numerical model. Therefore, further work on the nanowire attachment to the indenter tip is required.

It should be noticed that only the experimental $u_1/l - u_2/l$ curve of nanowire a intersects the theoretical curve for this nanowire (for $u_1/l = 0.313$).

However, in the case of nanowires b and c, the mid-span deflection was increasing until the end of the buckling test. There is a more significant difference between the mid-span deflection of nanowire a and nanowire b than between nanowire b and nanowire c. That happened due to the difference in the aspect ratio of nanowires. Nanowires with a relatively minor aspect ratio, which equals the ratio of length to nanowire diameter, may undergo shell buckling rather than column (Euler) buckling [11]. Feliciano *et al*. report no column buckling for carbon nanotube aspect ratio ~ 7. However, for $l/d \sim 20$, Euler buckling occurs [25]; therefore, mid-span deflection for nanowires is much smaller than for the other tested nanowires with an aspect ratio above 20.

The deflection values regarding nanowire b and nanowire c were higher than expected from the theoretical analysis. It might be due to simplifications applied in this model. The model assumes that the rod is incompressible but slightly compressed. Normal and shearing forces are neglected, although they occur in reality. We present an elastic approach; nevertheless, generally, the plastic effects can also appear.

The deformation has to possess specific regularity properties. Furthermore, discontinuous deformation would correspond to a fracture, indicating a need to complement the model and consider more important factors, such as scale effect or surface energy.

Figure 5 illustrates the difference in theoretical and experimental values of mid-span deflection. The difference between experimental and theoretical results is the lowest for nanowire with the smallest aspect ratio. During the first half of the compression, the error is positive, and then it begins to decline, reaching the negative value. However, it may indicate model instability. For example, concerning nanowires b and c, the difference between experiment and theoretical mid-span deflection values increased at the beginning of compression and then slowly declined.

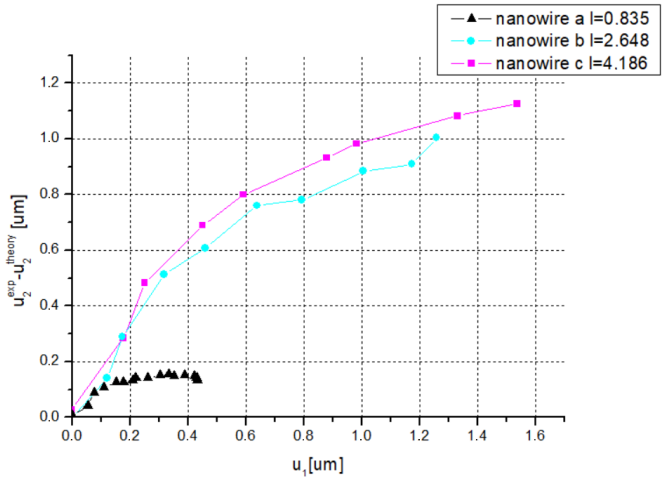

Fig. 5. The difference in theoretical and experimental values of the mid-span deflection

In Figure 6, three buckling configurations have been represented. The deformed elastic lines have been plotted using

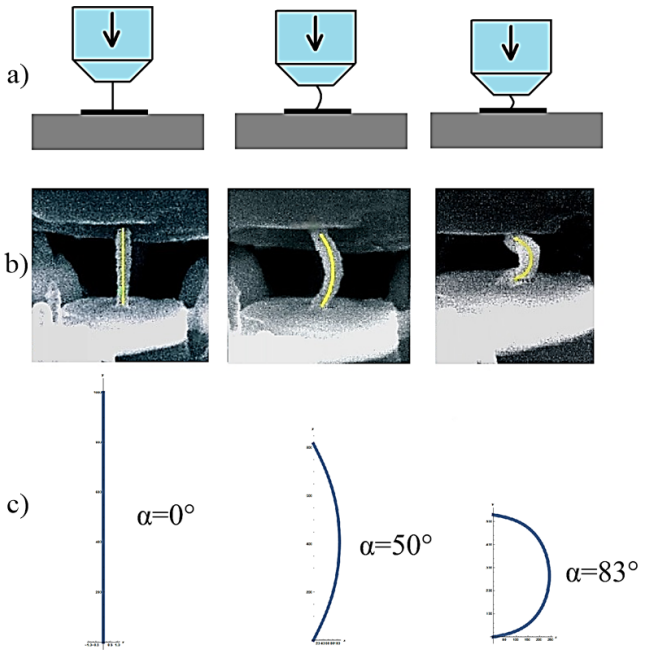

Fig. 6. Three buckling stages: a) scheme of compression of a single nanowire with the use of a flat tip nanoindenter b) SEM images with marked predicted deformed elastic lines (yellow lines) c) elastic lines by Wolfram Mathematica for given initial angle of the nanowire, respectively $\alpha = 0°$, $\alpha = 50°$ and $\alpha = 83°$

Wolfram Mathematica Software for three values of the initial angle of inclination α and marked on the images of a nanowire captured inside an SEM chamber. The values of α angle were measured from the SEM images and implemented to the Mathematica as specific values, namely, $\{0°, 50°, 83°\}$. The elastica for given m and α can be plotted using equations (3) and (4). In this analysis, the span lengths and diameters of nanowires were the same as measured. According to the previous reports, [26] $E = 75$ GPa gives Young's modulus mechanical properties in this simulation. The experiment results demonstrated a pretty good agreement with those plotted in Mathematica.

However, it should be noted that in real boundary conditions the case corresponds partially to simply supported beam and double clamp. In this paper, the simply supported, double-pinned beam is considered. In the case of double clamp boundary conditions, the equations describing the deformed shape of elastica differ [29]. In further studies, the mixed boundary conditions should be taken into account.

5. CONCLUSIONS

Based on the nonlinear elasticity theory, this research studied the post-buckling behaviour of simply supported nanowires. Nanowires with various length-to-diameter ratios were examined, and the effect of geometrical parameters was discussed. The results demonstrated that the mid-span deflection increases by increasing the length-to-diameter ratio. Also, it is observed that the displacement of the end of the nanowire is aspect-ratio dependent. It was shown that, in general, Euler's Buckling Formula should apply in predicting the shape of elastica (Fig. 5). Still, it needs to be improved concerning calculating the exact deflection value in the nanoscale.

ACKNOWLEDGEMENTS

The present research was partially supported by the Polish National Science Centre, 2021/43/B/ST8/02895.

REFERENCES

[1] V.G.A. Goss, "The history of the planar elastica: insights into mechanics and scientific method," *Sci. Educ.*, vol. 18, no. 8, pp. 1057–1082, 2009, doi: 10.1007/s11191-008-9166-2.

[2] S. Matsutani, "Euler's elastica and beyond," *J. Geom. Symmetry Phys.*, vol. 17, pp. 45–86, 2010, doi: 10.7546/jgsp-17-2010-45-86.

[3] S. Deshpande, "Buckling and post buckling of structural components," M.S. thesis, The University of Texas at Arlington, 2010. [Online]. Available: https://search.proquest.com/openview/1ec9e5d3c1d9eb0faf2639416b7b4743/1?pq-origsite=gscholar&cbl=18750, [Accessed: 24 Feb. 2022].

[4] J. Coyne, "Analysis of the formation and elimination of loops in twisted cable," *IEEE J. Oceanic Eng.*, vol. 15, no. 2, pp. 72–83, 1990, doi: 10.1109/48.50692.

[5] Ü. Sönmez, "Synthesis methodology of a compliant exact long dwell mechanism using elastica theory," *Int. J. Mech. Mater. Des.*, vol. 3, pp. 73–90, 2006, doi: 10.1007/s10999-006-9014-y.

[6] H.H. Hilton and S.J. D'Urso, "Designer Euler and elastica columns subjected to aerodynamic loads-system engineering of the aeroelasticity of wind turbine towers", *54th AIAA/ASME/ASCE/AHS/ASC Structures, Structural Dynamics, and Materials Conference*, 2013, doi: 10.2514/6.2013-1821.

[7] V. Goss and R. Chaouki, "Loading paths for an elastic rod in contact with a flat inclined surface," *Int. J. Solids Struct.*, vol. 88–89, pp. 274–282, 2016, doi: 10.1016/j.ijsolstr.2016.02.042.

[8] H. Yoshihara and M. Maruta, "Critical load for buckling of solid wood elements with a high slenderness ratio determined based on elastica theory", *Holzforschung*, vol. 76, no. 2, pp. 179–187, 2022, doi: 10.1515/hf-2021-0108.

[9] P.A. Djondjorov, M.T. Hadzhilazova, I.M. Mladenov, and V.M. Vassilev, "Explicit parameterisation of Euler's elastica," *Proc. of the Ninth International Conference on Geometry, Integrability and Quantisation. (Geometry, Integrability and Quantization, Proceedings Series)*, Bulgaria, pp. 175–187, 2008, doi: 10.7546/giq-9-2008-175-186.

[10] A. Balaeff, L. Mahadevan and K. Schulten, "Modeling DNA loops using the theory of elasticity," *Phys. Rev. E*, vol. 73, p. 031919, 2006, doi: 10.1103/PhysRevE.73.031919.

[11] A.A. Travers and J.M.T. Thompson, "An introduction to the mechanics of DNA," *Philos. Trans. R. Soc. A-Math. Phys. Eng. Sci.*, vol. 362, pp. 1265–1279, 2004, doi: 10.1098/rsta.2004.1392.

[12] H. Shima, "Buckling of carbon nanotubes: A state of the art review," *Materials*, vol. 5, no. 1, pp. 47–84, 2011, doi: 10.3390/ma5010047.

[13] H.W. Yap, R.S. Lakes, and R.W. Carpick, "Mechanical instabilities of individual multiwalled carbon nanotubes under cyclic axial compression," *Nano Lett.*, vol. 7, no. 5, pp. 1149–1154, 2007, doi: 10.1021/nl062763b.

[14] A. Muc and A. Banaś, "Eigenproblems in nanomechanics", *Bull. Pol. Acad. Sci. Tech. Sci*, vol. 63, no 3, pp. 819–25, 2015.

[15] T. Kuzumaki and Y. Mitsuda, "Nanoscale mechanics of carbon nanotube evaluated by nanoprobe manipulation in transmission electron microscope," *Jpn. J. Appl. Phys.*, vol. 45, no. 1A, pp. 364–368, 2006, doi: 10.1143/jjap.45.364.

[16] V.V. Dobrokhotov, M.M. Yazdanpanah, S. Pabba, A. Safir, and R.W. Cohn, "Visual force sensing with flexible nanowire buckling springs," *Nanotechnology*, vol. 19, no. 3, p. 35502, 2008, doi: 10.1088/0957-4484/19/03/035502.

[17] S. Pathak, Z.G. Cambaz, S.R. Kalidindi, J.G. Swadener, and Y.Gogotsi, "Viscoelasticity and high buckling stress of dense carbon nanotube brushes," *Carbon*, vol. 47, no. 8, pp. 1969–1976, 2009, doi: 10.1016/j.carbon.2009.03.042.

[18] J. Aizpurua, G.W. Bryant, L.J. Richter, F.J. García de Abajo, B.K. Kelley, and T. Mallouk, "Optical properties of coupled metallic nanorods for field-enhanced spectroscopy," *Phys. Rev. B*, vol. 71, no. 23, p. 235420, 2005, doi: 10.1103/physrevb.71.235420.

[19] R. Krahne, L. Manna, G. Morello, and A. Figuerola, *Physical properties of nanorods*. NanoScience and Technology series, Springer Berlin, Heidelberg, 2013, doi: 10.1007/978-3-642-36430-3.

[20] A. Machín *et al.*, "One-Dimensional (1D) nanostructured materials for energy applications," *Materials*, vol. 14, no. 10, p. 2609, May 2021, doi: 10.3390/ma14102609.

[21] X. Li, L. Li, Y. Hu, Z. Ding, and W. Deng, "Bending, buckling and vibration of axially functionally graded beams based on nonlocal strain gradient theory," *Compos. Struct.*, vol. 165, pp. 250–265, 2017, doi: 10.1016/j.compstruct.2017.01.032.

[22] N.A.C. Sidik, M.N.A.W.M. Yazid, and S. Samion, "A review on the use of carbon nanotubes nanofluid for energy harvesting system," *Int. J. Heat Mass Transf.*, vol. 111, pp. 782–794, 2017, doi: 10.1016/j.ijheatmasstransfer.2017.04.047.

[23] I.F. Golovnev, E.I. Golovneva, and A.V. Utkin, "Effect of the Nanorod Size on Energy Absorption at the Microlevel under Cyclic Loading," *Phys. Mesomech.*, vol. 22, no. 5, pp. 420–431, 2019, doi: 10.1134/S1029959919050084.

[24] A.R. Setoodeh, M. Khosrownejad, and P. Malekzadeh, "Exact nonlocal solution for postbuckling of single-walled carbon nanotubes," *Physica E*, vol. 43, no. 9, pp. 1730–1737, 2011, doi: 10.1016/ j.physe.2011.05.032.

[25] C. Thongyothee and S. Chucheepsakul, "Postbuckling behaviors of nanorods including the effects of nonlocal elasticity theory and surface stress," *J. Appl. Phys.*, vol. 114, no. 24, p. 0243507, 2013, doi: 10.1063/1.4829896.

[26] D. Bigoni, *Nonlinear Solid Mechanics: Bifurcation Theory and Material Instability*, Cambridge: Cambridge University Press, 2012.

[27] J. Feliciano, C. Tang, Y. Zhang, and C. Chen, "Aspect ratio dependent buckling mode transition in single-walled carbon nanotubes under compression," *J. Appl. Phys.*, vol. 109, no. 8, p. 084323, 2011, doi: 10.1063/1.3569616.

[28] L. Philippe, B. Cousin, Z. Wang, D.F. Zhang, and J. Michler, "Mass density of individual cobalt nanowires," *Appl. Phys. Lett.*, vol. 96, no. 5, p. 51903, 2010, doi: 10.1063/1.3299013.

[29] D. Bigoni, F. Bosi, D. Misseroni, F. Dal Corso, and G. Noselli, "New phenomena in nonlinear elastic structures: from tensile buckling to configurational forces" in *Extremely Deformable Structures*, CISM Lecture Notes No. 562, Springer, 2015, pp. 55–137, doi: 10.1007/978-3-7091-1877-1.